The Mechanism of VWF-Mediated Platelet GPIbα Binding

Matthew Auton,[†] Cheng Zhu,[‡§] and Miguel A. Cruz[†*]
[†]Cardiovascular Research, Baylor College of Medicine, Houston, Texas; and [‡]Woodruff School of Mechanical Engineering, [§]Coulter Department of Biomedical Engineering, Georgia Institute of Technology, Atlanta, Georgia

ABSTRACT The binding of Von Willebrand Factor to platelets is dependent on the conformation of the A1 domain which binds to platelet GPIbα. This interaction initiates the adherence of platelets to the subendothelial vasculature under the high shear that occurs in pathological thrombosis. We have developed a thermodynamic strategy that defines the A1:GPIbα interaction in terms of the free energies (ΔG values) of A1 unfolding from the native to intermediate state and the binding of these conformational states to GPIbα. We have isolated the intermediate conformation of A1 under nondenaturing conditions by reduction and carboxyamidation of the disulfide bond. The circular dichroism spectrum of reduction and carboxyamidation A1 indicates that the intermediate has ~10% less α-helical structure that the native conformation. The loss of α-helical secondary structure increases the GPIbα binding affinity of the A1 domain ~20-fold relative to the native conformation. Knowledge of these ΔG values illustrates that the A1:GPIbα complex exists in equilibrium between these two thermodynamically distinct conformations. Using this thermodynamic foundation, we have developed a quantitative allosteric model of the force-dependent catch-to-slip bonding that occurs between Von Willebrand Factor and platelets under elevated shear stress. Forced dissociation of GPIbα from A1 shifts the equilibrium from the low affinity native conformation to the high affinity intermediate conformation. Our results demonstrate that A1 binding to GPIbα is thermodynamically coupled to A1 unfolding and catch-to-slip bonding is a manifestation of this coupling. Our analysis unites thermodynamics of protein unfolding and conformation-specific binding with the force dependence of biological catch bonds and it encompasses the effects of two subtypes of mutations that cause Von Willebrand Disease.

INTRODUCTION

Von Willebrand Factor (VWF) is a main responder to vascular injury, and functions to sequester and adhere platelets to the subendothelium and initiate coagulation (1). VWF is a multidomain glycoprotein consisting of multiple copies of A, B, C, and D type domains that is secreted into the blood as a large multimeric polymer from vascular endothelial cells and activated platelets (2). The interaction between VWF and platelets is mediated by the A1 domain, which binds platelet glycoprotein (GP)Ibα under conditions of high shear in the vasculature where primary hemostasis is absolutely dependent on VWF (3,4).

It has been postulated that VWF undergoes a conformational change, such that it activates VWF to promote the exposure of the cryptic binding site, and thus, enable GPIbα to effectively bind to platelets. This process of unfurling multimeric VWF is enhanced by the hydrodynamic forces of elevated shear stress that occur at sites of vascular injury (5,6). Apparently, the intrinsic conformation of the A1 domain remains intact during the structural change of VWF because the bond strength formed between GPIbα and isolated A1 domain is identical to that determined for ultra-large VWF multimers, which expose, constitutively, the binding site for GPIbα (7). However, the interaction between platelets and VWF is not simply dependent only on the shear-induced exposure of the A1 domain to GPIbα. The efficiency of platelet adherence is also dependent on the strength of the tethering forces occurring between A1 and GPIbα, which is strongly correlated to the stability of the A1 domain (8).

By using thermodynamic approaches, we have shown that the A1 domain unfolds in a three-state manner through an intermediate state between the fully folded native state and the unfolded denatured state (8). Clinical Von Willebrand disease (VWD) mutations in the A1 domain that result in a gain of function phenotype (the VWD type 2B mutations, R1306Q and I1309V), shift the $N \rightleftharpoons I$ equilibrium in favor of the intermediate state. Conversely, mutations that cause loss of function (such as the VWD type 2M mutation, G1324S) stabilize the native state. The thermodynamic effects of these mutations are correlated to the force-dependent catch-slip bonding between A1 and GPIbα in which the equilibrium bond lifetime and critical force vary in proportion to the thermodynamic stability of A1 (9). Catch-bonding between two proteins is characterized by an increased lifetime of the interaction in the presence of mechanical tensile force. After a threshold critical force is reached, the interaction transitions to a slip-bond where increasing tensile forces decrease the lifetime of the interaction. This force-sensing binding process regulates platelet-rolling velocities on VWF in the presence of vascular shear stress (8,10). These results suggest that the intermediate state may represent the high-affinity GPIbα-binding conformation that occurs during high shear stress in the vasculature.

In this study, we have effectively isolated the intermediate conformation of A1 by reducing and carboxyamidating the

Submitted March 5, 2010, and accepted for publication June 1, 2010.

*Correspondence: miguelc@bcm.tmc.edu

Editor: Patricia L. Clark.

0006-3495/10/08/1192/10 $2.00

doi: 10.1016/j.bpj.2010.06.002

disulfide bond. This protein modification results in an increased affinity for platelet GPIbα, demonstrating for the first time that binding and unfolding are thermodynamically coupled. In light of this new information about the conformational dependence of binding, we revisit the catch-slip bonding between clinical variants of A1 and platelet GPIbα and develop a model that integrates both the thermodynamic and the force-dependent adhesion properties that characterize this interaction.

METHODS

Protein expression, purification, and chemical modification

Recombinant wild-type (WT), R1306Q, I1309V, and G1324S VWF-A1 (amino acids Q_{1238} - P_{1471}) domain variants were purified as previously described (3,11). The A1 domain was dialyzed against 10 mM NaAcetate, 10 mM Phosphate, 10 mM Glycine, 150 mM NaCl, and 2 mM EDTA, pH = 8 and stored on ice until experimentation. Reduction and carboxyamidation of the A1 domain (RCAM A1) was done in a similar manner to Qu et al. (12) using dithiothreitol (DTT) and iodoacetamide (IAA). A 1-mL portion of purified A1 domain was dialyzed against buffer containing 2 M Guanidine HCl. After dialysis, the protein solution was added to a tube containing a preweighed amount of DTT so that the molarity of DTT = 6 mM. This mixture was allowed to react for 3 h under nitrogen to reduce the disulfide bond in A1. After reduction, the mixture was transferred to a second tube containing a preweighed amount of IAA so that the molarity of IAA = 12 mM. This mixture was allowed to react in the dark for 1 h and the reaction was quenched by adding 10 μL of β-mercaptoethanol (β-ME). RCAM A1 was extensively dialyzed against buffer containing 2 M guanidine HCl (GndHCl) to removed excess DTT and IAA and stored on ice until experimentation. The purity of both WT and RCAM A1 was determined by sodium dodecyl sulfate polyacrylamide gel electrophoresis (SDS-PAGE) and quantified by ultraviolet (UV) absorption at 280 nm on a model No. DU UV-Vis spectrophotometer (Beckman Coulter, Fullerton, CA) as previously described using the method of Pace et al. (13). A quantity of 10 μM WT A1, RCAM A1, and bovine serum albumin were applied to a model No. SEC S3000 size exclusion column (7.8 × 300 mm; Phenomenex, Torrance, CA) using a Sprint perfusion chromatography system (BioCad, Moscow, Russia). The mobile phase (phosphate-buffered saline) was delivered at a flow rate of 1 mL/min, and detection was by UV absorbance at 280 nm.

Analysis of secondary structure content in WT and RCAM A1

Using the structural coordinate data of WT A1 (Protein Databank ID = 1auq), the secondary structure content was calculated using the Dictionary of Protein Secondary Structure (DSSP), a pattern-recognition process of hydrogen-bonded and geometrical features extracted from x-ray coordinates (14), and protein secondary structure (PROSS), a dihedral angle-based secondary structure assignment algorithm (http://www.roselab.jhu.edu/utils/pross.html). These algorithms output the per-residue secondary structure content in terms of α-helix, β-strand, turns, polyproline II, and random coil (DSSP combines turns with polyproline II). The number of residues classified into each secondary structure class were summed and then divided by the total number of residues in the A1 domain structure to obtain the percent of each secondary structure type. Turns, polyproline II, and random coil were combined as a remainder of secondary structure that is not α-helix or β-strand.

From the circular dichroism spectra of WT A1 and RCAM A1, we used the algorithm, circular dichroism secondary structure (CDSSTR) (15), part of the CDPro software package (http://lamar.colostate.edu/sreeram/CDPro/main.html), to deconvolute the spectra into percent α-helix, β-strand, turns, and random coil secondary structure content. CDSSTR extracts secondary structure content from a user-provided spectrum using a singular value decomposition algorithm on a reference set of proteins for which CD spectra and x-ray coordinate data are known. We used the SDP48 reference set, which contains 43 soluble proteins and five denatured proteins (16). This algorithm outputs the percent regular and distorted α-helix, the percent β-strand content, and the percent turn and random coil content. Distorted helical content results from less-ordered residues on the N- or C-terminus of α-helices as described by Sreerama et al. (17); therefore, we group the distorted helical content with that of turns and random coils into the remainder of secondary structure that is not regular α-helix or β-strand.

A1 domain binding to fixed lyophilized platelets

Platelet-binding assays were performed using enzyme-linked immunosorbent assay (ELISA) as we have described (18). Briefly, all incubations were 1 h at 37°C in microtiter wells coated with lyophilized fixed platelets. Stock solutions of WT, R1306Q, I1309V, G1324S, and RCAM A1 domain were quantified by UV spectroscopy before experiment, and serial dilutions into TBS solution (TBS Technologies, Holliston, MA) were made to obtain the desired final protein concentration. For RCAM A1, the concentration of GndHCl never exceeded 0.2 M at the highest protein concentration of 10 μM, and UV spectroscopy did not reveal any light scattering due to RCAM aggregation. We obtained ~95% saturation in the RCAM binding curve at 1 μM corresponding to only 0.02 M GndHCl, which is comparable to the buffer concentration. Furthermore, within the concentration range of RCAM binding (0.005−1 μM), the GndHCl content was negligible. Residual-bound A1 domain was detected with peroxidase-conjugate monoclonal anti-His antibody. The binding data were normalized on a fraction-bound scale to eliminate uncertainties in the amount of platelets immobilized on the microtiter wells from multiple experiments and to directly compare the binding affinities. Further specificity of RCAM A1 binding, evaluated in the presence of 0.12 μM RCAM A1 (~1/2 saturation) and a 10-fold excess (1.2 μM) of the monoclonal antibody against GPIb (6D1), averaged 40 ± 13% inhibition, consistent with previous determinations with WT A1 (19).

RESULTS

Structural characterization of RCAM A1 relative to WT A1

In Fig. 1 *A*, size exclusion chromatography was performed using a model No. SEC S3000 column (Phenomenex) to verify that reduced and carboxyamidated (RCAM) A1 remained soluble and monomeric, as shown previously for WT A1 (19). Both WT and RCAM at a concentration of 10 μM eluted as a single peak at (V_E = 10.4 mL) and (V_E = 13.1 mL), respectively. To verify that the disulfide bond is effectively blocked, SDS-PAGE confirms that the relative mobility of RCAM A1 under nonreducing conditions is identical to both WT A1 and RCAM A1 in the presence of β-mercaptoethanol (*inset* of Fig. 1 *A*).

Fig. 1 *B* compares the far-UV circular dichroism spectra of both WT and RCAM A1. Reduction and carboxyamidation of the disulfide bond in the A1 domain blocks the disulfide and prevents the disulfide from reoxidizing. This chemical modification results in a significant loss in secondary structure relative to the disulfide intact

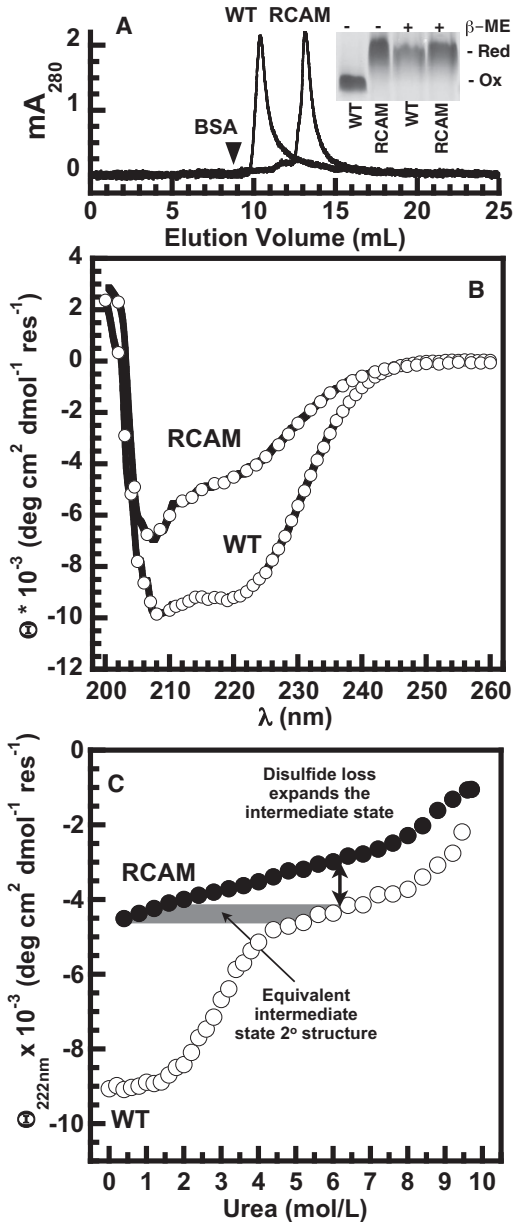

FIGURE 1 (*A*) Size exclusion chromatography of 10 μM WT and RCAM A1. Elution volume of bovine serum albumin (molecular mass = 68 kDa) indicated by arrowhead. (*Inset*) Nonreducing (− β-ME) and reducing (+ β-ME) SDS-PAGE of WT and RCAM A1. (*B*) Far-UV CD spectra of 10 μM WT and RCAM A1 in the presence of 0.5 M urea. Spectra represent the average of 10 individual scans with a pathlength of 1 mm at 25°C. (*C*) Urea unfolding of WT and RCAM A1 monitored at 222 nm.

WT A1; however, it does not cause A1 to become completely unfolded. RCAM A1 retains secondary structure, as is evident by the 208-nm minimum and the residual ellipticity at 222 nm.

As described in the Methods, the CDSSTR algorithm was used to deconvolute the CD spectra of WT and RCAM A1 into their respective α-helical, β-strand, and remaining less-ordered secondary structure content. Table 1 shows that the secondary structure content of WT A1 derived from the spectral deconvolution and the actual secondary structure content derived from the x-ray coordinate data using PROSS and DSSP are in agreement. Compared to WT A1, the spectral deconvolution of RCAM A1 shows a loss of ~10% α-helix and a gain of an equivalent amount in the remaining less-ordered random coil structure.

To further investigate these structural differences, Fig. 1 *C* compares the urea unfolding of RCAM A1 to the disulfide-bond-intact WT A1 domain. While the WT A1 has the characteristic native to intermediate transition from 0 to 5 M urea previously published (8,9), at low urea concentrations (0–1 M) where WT A1 is fully folded, RCAM A1 has a secondary structure consistent with the intermediate state of WT A1 in the presence of urea. At higher urea concentrations, RCAM A1 expands relative to the disulfide intact WT A1 due to the increased conformational degrees of freedom associated with loss of the disulfide bond. The cumulative results of Fig. 1 indicate that the disulfide bond is required for folding to the native structure, and removing the disulfide induces the intermediate conformation of A1, which contains 10% less α-helical content under non-denaturing conditions.

A1 domain binding to platelets

Reduction and carboxyamidation of the disulfide bond effectively isolates the intermediate conformation of the A1 domain and this provides a means to test the conformational dependence of A1 domain binding to platelet GPIbα. Fig. 2 compares the equilibrium binding of WT, R1306Q, I1309V, G1324S, and RCAM A1 to lyophilized fixed platelets at 37°. RCAM A1 binds GPIbα with high affinity, R1306Q and I1309V bind with medial affinity, and WT and G1324S bind with low affinity. Within the error of the ELISA technique, the binding affinities of R1306Q and I1309V are nearly indistinguishable, as are the affinities of WT and G1324S; however, the apparent affinities correlate with the thermodynamic stability of these variants.

Previously, we determined the thermodynamics of unfolding of the A1 domain using the urea-temperature phase diagram method, which provided the free energy of unfolding from $N \rightleftharpoons I$ as a function of temperature (8). Combining our previous studies on unfolding with the binding results obtained here permits a description of the A1:GPIbα interaction in the context of the thermodynamic framework shown in Fig. 3, as derived in the Supporting Material. In the thermodynamic cycle, the horizontal equilibria represent the intrinsic binding free energies of the A1 domain native and intermediate conformations to platelet GPIbα, ΔG^0_{NG}, and ΔG^0_{IG}, respectively. The vertical equilibrium on the left of the thermodynamic cycle is the free energy of unfolding the A1 domain, $\Delta G^0_{N\rightleftharpoons I}$ given in Table 2, which we previously quantified (8). The vertical equilibrium on the right of the thermodynamic cycle represents the free energy of conformational change within the bound complex,

TABLE 1 Secondary structure content of WT A1 and RCAM A1

	WT	WT	WT	WT	RCAM	RCAM-WT
Method*	PROSS	DSSP	CDSSTR	Average†	CDSSTR	Difference‡
% α-Helix	35	37	34	35 ± 2	25	−10
% β-Sheet	21	22	22	22 ± 1	22	0
% Remainder§	44	41	44	43 ± 2	53	+10

*PROSS and DSSP calculate the secondary structure content from the WT A1 crystal coordinate data (Protein DataBank ID = 1auq) and CDSSTR predicts the secondary structure content from the CD spectra of Fig. 1 *B*.
†Average of columns 2–4.
‡Difference between columns 5 and 6.
§Remaining structure contains contributions from β-turns, polyproline II, and random coil structure.

$\Delta G^0_{NG\rightleftharpoons IG}$. Based on this thermodynamic cycle, the partition function, Q, with respect to the total concentration of A1, $[A1]$ (abscissa of Fig. 2) is

$$Q = K1 + K2[A1], \tag{1}$$

where $K1 = 1 + K_{N\rightleftharpoons I}$ and $K2 = K_{NG} + K_{IG}K_{N\rightleftharpoons I}$ are functions of the equilibrium constants for A1 unfolding from $N \rightleftharpoons I$ and the intrinsic binding affinities for the native and intermediate states, K_{NG} and K_{IG}. This partition function is valid when the total concentration of A1 is in large excess over the total concentration of GPIbα as is the case for our ELISA binding assay. The apparent binding affinity is given by the ratio, $K_b^{app} = K2/K1$, and from the partition function, the degree of binding provides the basic equation for fitting the data shown in Fig. 2,

$$X = \frac{K2 * [A1]}{K1 + K2[A1]}. \tag{2}$$

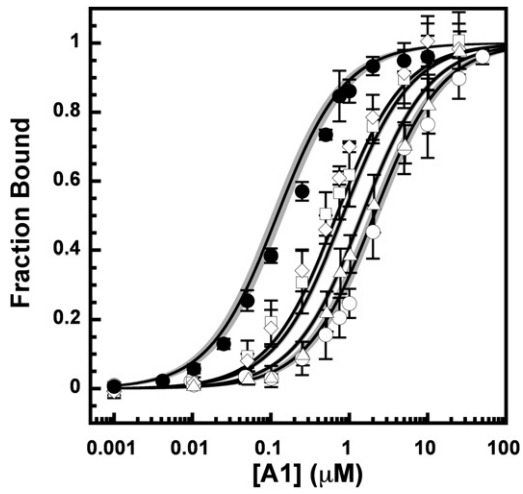

FIGURE 2 The binding of WT (*circles*), R1306 (*squares*), I1309V (*diamonds*), G1324S (*triangles*), and RCAM A1 domain (*solid circles*) to fixed platelets at 37°C. Data are representative of three experiments each done in triplicate. (*Error bars*) Standard deviation of the mean. (*Lines*) Best fit. (*Shaded areas*) Representative of the fitting error. The binding affinities reported in Table 2 were obtained by fitting the data to Eq. 2 weighted according to the error on each data point.

Globally fitting Eq. 2 to the data shown in Fig. 2 gives the intrinsic binding affinities of the native and intermediate states of A1 (Table 2). Within the error of the ELISA technique, the binding curves resulting from Eq. 2 agree remarkably well with the experimental data and demonstrate that the change in binding affinity is directly coupled to the conformational equilibrium between the native and intermediate states of A1. The intrinsic binding affinity of the intermediate state ($K_{IG} = (8.3 \pm 0.8) \times 10^6\ M^{-1}$) has ~20-fold tighter binding affinity than the native state ($K_{NG} = (0.48 \pm 0.06) \times 10^6\ M^{-1}$). The free energy of binding is

$$\Delta G_b^0 = -RTln\, K_b^{int},$$

where K_b^{int}, the state specific binding affinity, has the units (μM^{-1}), R is the gas constant (0.001987 kcal mol^{-1} K^{-1}), and the temperature is $T = 310$ K at 37°C (Table 2). A resulting consequence of the thermodynamic cycle is the following relationship that equates the binding free energy contributions to the free energies associated with unfolding and conformational change,

$$\Delta G^0_{IG} - \Delta G^0_{NG} = \Delta G^0_{NG\rightleftharpoons IG} - \Delta G^0_{N\rightleftharpoons I}. \tag{3}$$

Given the native and intermediate state intrinsic binding affinities determined from Fig. 2 and the $N \rightleftharpoons I$ unfolding free energies determined previously (8), we can readily solve for the free energy of conformational change in the A1:GPIbα complex, $\Delta G^0_{NG\rightleftharpoons IG}$, using Eq. 3. The results of Eq. 3 for WT A1 and three VWD clinical variants of the A1 domain are given in Table 3. The equilibrium stability

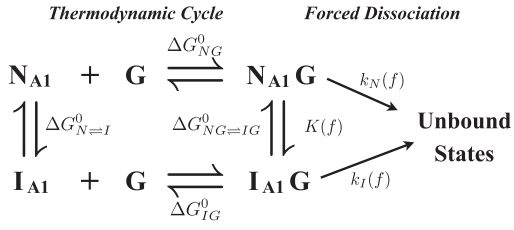

FIGURE 3 Thermodynamic cycle defining the equilibrium binding of A1 to GPIbα and the catch-to-slip bond model of forced dissociation from two bound conformational states.

TABLE 2 The apparent binding affinity (K_b^{app}) and stability ($\Delta G^0_{N\rightleftharpoons I}$) of the A1 domain variants and the native and intermediate state specific intrinsic binding affinity (K_{NG} and K_{IG}) and free energy (ΔG^0_{NG} and ΔG^0_{IG}) at 37°C

A1 Variant	K_b^{app}*	$\Delta G^0{}_{N\rightleftharpoons I}$†
VWD type	$\times 10^6$ M^{-1}	kcal/mol
WT (normal)	0.69 ± 0.03	2.20 ± 0.18
R1306Q (2B)	1.46 ± 0.02	1.20 ± 0.12
I1309V (2B)	1.21 ± 0.03	1.40 ± 0.11
G1324S (2M)	0.48 ± 0.06	4.30 ± 0.14
RCAM	8.3 ± 0.8	$\lesssim -5$
Thermodynamic	K_b^{int}‡	ΔG_b^{0}‡
State	$\times 10^6$ M^{-1}	kcal/mol
Native	0.48 ± 0.06	0.45 ± 0.08
Intermediate	8.3 ± 0.8	−1.31 ± 0.09

*$K^{b}_{app} = K2/K1$ as described in the text.
†Reported by us in Auton et al. (8).
‡K^{b}_{int} represents the state specific binding affinities, K_{NG} and K_{IG}, and $\Delta G^0_b = -RT\ln K^{tb}_{in}$.

of the complex between GPIbα and WT A1 is 0.4 ± 0.2 kcal/mol, which means that the native bound conformation of WT A1 is slightly more favored than the intermediate bound conformation. Depending on the effect of clinical mutations on A1 domain stability, $\Delta G^0_{NG\rightleftharpoons IG}$ can change sign and favor the intermediate bound conformation, as is the case for both of the type 2B variants, R1306Q and I1309V (see Table 3). The significance of this thermodynamic relationship is that it predicts that the bound complex between the A1 domain and GPIbα consists of an equilibrium between low-affinity and high-affinity bound states. Furthermore, $\Delta G^0_{NG\rightleftharpoons IG}$ should be sensitive to the hydrodynamic forces that occur in circulation as a result of platelet tethering to VWF. Knowledge of the thermodynamic stability of the A1:GPIbα complex makes possible the quantitative description of the force-dependent catch-to-slip binding that we previously observed using atomic force microscopy (10).

Catch-to-slip bonds revisited

Given the thermodynamic cycle comprised of A1 domain unfolding, A1 binding to GP1bα, and conformational change within the bound A1:GP1bα complex shown in Fig. 3, we consider a simplistic interpretation of the force dependence of catch-to-slip bonding. Our mechanism (derived in the Supporting Material) involves forced unbinding from two bound conformational states, $N_{A1}G$ and $I_{A1}G$, in an initial force-free thermodynamic equilibrium with a stability, $\Delta G^0_{NG\rightleftharpoons IG}$. An inherent assumption in our analysis is that the equilibrium rates of dissociation (k_i^0) exceed the equilibrium rates of interconversion ($k^0_{NG\rightarrow IG}$ and $k^0_{IG\rightarrow NG}$) between the $N_{A1}G$ and $I_{A1}G$ states. Because we have determined the thermodynamic stability of the complex, the absolute values of the rates of interconversion between bound states are not required, as their ratio defines the equilibrium constant, $K^0 = k^0_{NG\rightarrow IG}/k^0_{IG\rightarrow NG}$. Both the equilibrium ($N_{A1}G \rightleftharpoons I_{A1}G$) and the rates of dissociation become force-dependent in Eqs. 4 and 5, according to the Bell model (20):

$$K(f) = K^0 \exp\left(\frac{\sigma f}{k_B T}\right). \tag{4}$$

Note that

$$K^0 = \exp\left(-\Delta G^0_{NG\rightleftharpoons IG}/RT\right)$$

is the force-free equilibrium constant calculated from Eq. 3, and σ is the conformational compliance that describes the force dependence of the equilibrium constant. The value k_B is the Boltzmann constant and T is the temperature in Kelvin. The rate of dissociation as a function of force is described similarly as

$$k_i(f) = k_i^0 \exp\left(\frac{y_i f}{k_B T}\right), \tag{5}$$

where $i = N$ for the bound native state ($N_{A1}G$) and $i = I$ for the bound intermediate state ($I_{A1}G$) of A1 in complex with GP1bα. The value k_i^0 is the equilibrium rate of dissociation and y_i defines the force dependence of dissociation.

TABLE 3 Thermodynamic and kinetic parameters defining the equilibrium and force dependence of the A1:GPIbα binding interaction at 37°C

VWD type	Normal	2B	2B	2M
A1 variant	WT	R1306Q	I1309V	G1324S
Equilibrium thermodynamics				
$\Delta G^0_{NG\rightleftharpoons IG}$ (kcal/mol)	0.4 ± 0.2	−0.6 ± 0.2	−0.4 ± 0.2	2.5 ± 0.2
$K^0_{NG\rightleftharpoons IG}$	0.52 ± 0.098	2.65 ± 0.37	1.91 ± 0.25	0.017 ± 0.003
Force-dependent kinetics				
$\Delta G^0_{NG\rightleftharpoons IG}$ (kcal/mol)	0.5 ± 0.3	−0.7 ± 0.3	−0.4 ± 0.3	2.5 ± 0.1
$K^0_{NG\rightleftharpoons IG}$	0.4 ± 0.1	2.9 ± 1.0	1.8 ± 0.5	0.018 ± 0.008
σ(nm)	0.45 ± 0.04	0.31 ± 0.05	0.38 ± 0.05	0.51 ± 0.01
$k^0_{N,off}$ (s^{-1})	4.9 ± 0.6	2.0 ± 0.7	2.5 ± 0.3	8.6 ± 0.3
$k^0_{I,off}$ (s^{-1})	1.84 ± 0.03	1.81 ± 0.04	1.84 ± 0.03	1.82 ± 0.05
y_N(nm)	−0.23 ± 0.005	0.23 ± 0.005	−0.23 ± 0.005	−0.23 ± 0.005
y_I(nm)	0.039 ± 0.002	0.037 ± 0.002	0.035 ± 0.003	0.037 ± 0.002

At thermodynamic equilibrium in the absence of force, the population of bound conformations of the A1 domain are $P_N^0 = 1/(1 + K^0)$ and $P_I^0 = K^0/(1 + K^0)$. However, because the bound states, $N_{A1}G$ and $I_{A1}G$, equilibrate slowly compared to the rates of dissociation, we utilize the concept of flux, described by Thomas et al. (21), to define the force-free conditions according to the probability that binding occurs in state i, B_i^0. The principle of detailed balance requires that the flux for initial bond formation equals the unbinding flux for each state, $J_i^0 = P_i^0\, k_i^0$, and the probability of binding to state i in the absence of force is

$$\begin{aligned} B_N^0 &= \frac{J_N^0}{J_N^0 + J_I^0} = \frac{k_N^0}{k_N^0 + k_I^0 K^0} \\ B_I^0 &= \frac{J_I^0}{J_N^0 + J_I^0} = \frac{k_I^0 K^0}{k_N^0 + k_I^0 K^0} \end{aligned}. \tag{6}$$

B_N^0 and B_I^0 provide the initial conditions for solving the following differential rate equations for the binding probability as a function of time,

$$\partial B_N/\partial t = -K_N^0 B_N(t) \text{ and } \partial B_I/\partial t = -K_I^0 B_I(t),$$

the results of which are equivalent to the equations described by Thomas et al. (21) in the limit of slow rates of interconversion between bound states relative to the rates of dissociation:

$$\begin{aligned} B_N^0(t) &= \frac{k_N^0 \exp(-k_I^0 t)}{k_N^0 + k_I^0 K^0} \\ B_I^0(t) &= \frac{k_I^0 K^0 \exp(-k_I^0 t)}{k_N^0 + k_I^0 K^0} \end{aligned}. \tag{7}$$

The average bond lifetime $\langle \tau^0 \rangle$ is calculated from the probability distribution of lifetimes, which is the negative derivative of the total probability of binding, $B^0(t) = B_N^0(t) + B_I^0(t)$:

$$\begin{aligned} \langle \tau^0 \rangle(t) &= -\int t\left(B_N^0(t) + B_I^0(t)\right)dt = \tau_N^0(t) + \tau_I^0(t) \\ &= \frac{(1 + k_N^0 t)\exp(-k_N^0 t)}{k_N^0\left(k_N^0 + k_I^0 K^0\right)} + \frac{K^0(1 + k_I^0 t)\exp(-k_I^0 t)}{k_I^0\left(k_N^0 + k_I^0 K^0\right)} \end{aligned}. \tag{8}$$

The time dependence of the flux, binding probabilities, and bond lifetimes are scaled to force by first noting the force dependence of the equilibrium and rate constants and substituting Eqs. 4 and 5 into Eqs. 7 and 8. Second, the pulling force is directly proportional to time via the loading rate, $f(t) = r_f t$. The loading rate, r_f, is a product of the rate of retraction ($v = 250$ nm/s) of the atomic force microscopy cantilever and the nominal cantilever spring constant ($k_c \simeq 10$ pN/nm). When rescaled to force, the functional form of Eqs. 7 and 8 is capable of describing proteins exhibiting catch-to-slip bond transitions as well as proteins that form only slip bonds, making it ideal for describing the force dependence of A1 binding to GPIbα, which does both.

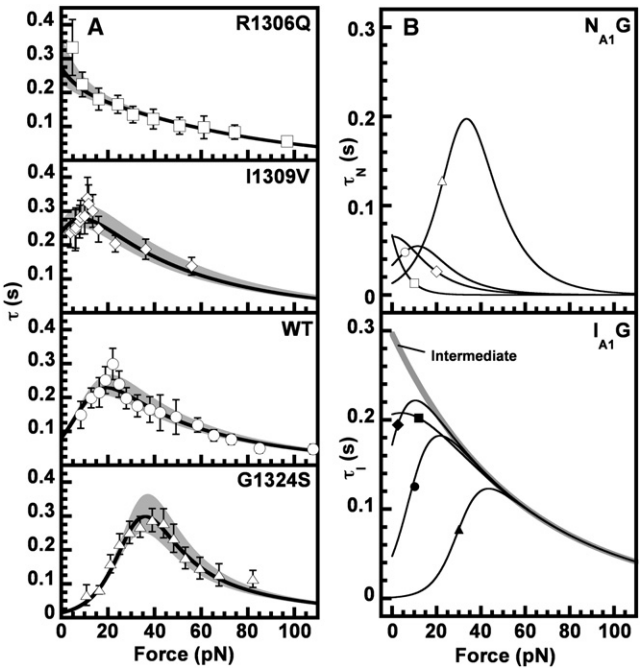

FIGURE 4 (*A*) Comparison of our previously reported catch-to-slip bond lifetime data as a function of force with the model fit to Eq. 8. (*Lines*) Best fit. (*Shaded areas*) Representative of the fitting error. (*B*) Deconvolution of the overall bond lifetime for each variant of the A1 domain into the native (τ_N) and intermediate (τ_I) state specific bond lifetimes as a function of force. (*Open symbols*) Native state. (*Solid symbols*) Intermediate state. (*Shaded curve*) Bond lifetime and the binding probability of the intermediate state. R1306Q (*squares*), I1309V (*diamonds*), WT (*circles*), and G1324S (*triangles*).

Fig. 4 *A* compares the results of fitting Eq. 8 to the experimental catch-to-slip bond data that we previously reported (8) for WT A1, and the type 2B (R1306Q and I1309V) and type 2M (G1324S) clinical variants that cause Von Willebrand disease. Table 3 gives the resulting kinetic parameters that describe the data. Equation 8 provides a remarkably good agreement with the experimental data, resulting in a root-mean-square of the residuals = 0.67 and a variance of the residuals = 0.45. The resulting parameters that define the force dependence of GPIbα binding to these A1 domain variants are given in Table 3.

An internal verification of the model is that fitting Eq. 8 to the lifetime data results in an equilibrium stability of the complex that, within error, agrees with what is obtained using the thermodynamic results of Eq. 3 (Table 3). This indicates that the overall bond lifetimes at zero force vary in proportion to the equilibrium stability of the complex. The conformational compliance, σ, slightly decreases with decreasing $\Delta G^0_{NG \rightleftharpoons IG}$, indicating that these mutations also

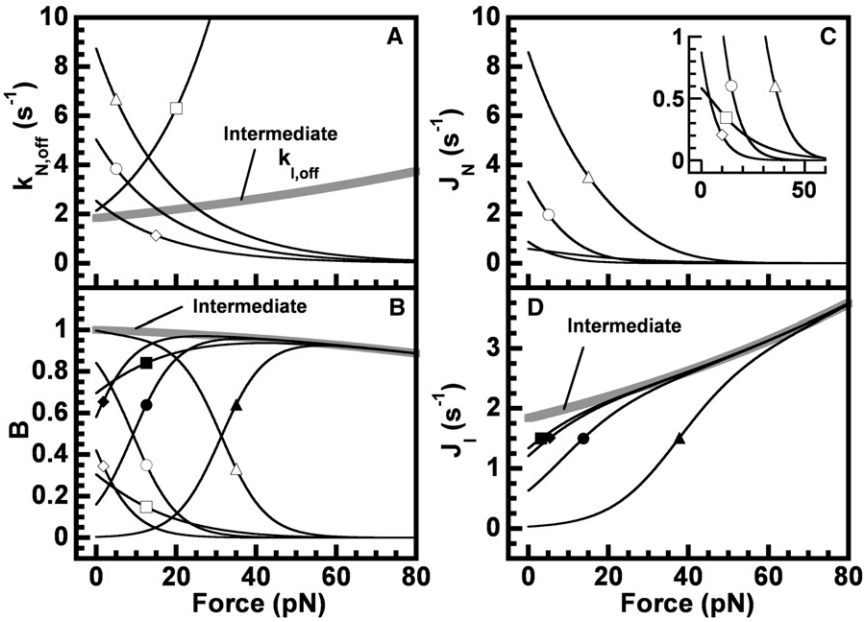

FIGURE 5 (*A*) Force dependence of the dissociation rates from the native and intermediate states. (*B*) Force dependence of the probability of binding (*B*) to each state. (*C* and *D*) Native and intermediate state flux as a function of force. (*C*, *inset*) Magnification of the J_N curves at <1 s^{-1}. (*A*, *B*, and *D*, *shaded curve*) Force dependence of the rate of dissociation (*A*), the binding probability (*B*), and the flux through the intermediate state (*D*). (*Open symbols*) Native state; (*solid symbols*) intermediate state for the A1 domain variants, R1306Q (*squares*), I1309V (*diamonds*), WT (*circles*), and G1324S (*triangles*).

have a moderate affect on the force dependence of the stability of the complex (Table 3).

In Fig. 4 *B*, we plot the $N_{A1}G$ and $I_{A1}G$ bound state specific lifetimes, τ_N and τ_I, as a function of force. The value τ_N is generally $<\tau_I$ except for the highly stable type 2M G1324S variant, where τ_N can exceed τ_I. The large τ_N at high stability is partly due to the fact that $K_0 \rightarrow 0$, but also because the rate of dissociation from the native state, $k_N \rightarrow 0$, is a function of force, as shown in Fig. 5. The force dependence of τ_I of all the A1 domain variants increases and approaches a common lifetime that represents the contribution of the intermediate state. Extrapolating τ_I at high force back to zero force in the limit as $K^0 \rightarrow \infty$ (i.e., the intermediate is 100% populated) gives the force dependence of the intermediate state bond lifetime, which begins at ~0.3 s and decays with force as a slip bond (*gray curve*). The force dependence of the intermediate state bond lifetime is what would be expected for RCAM A1.

In Fig. 5, we plot the state specific dissociation rates, binding probabilities, and flux. The A1 domain variants that form catch bonds with GPIbα all exhibit native state dissociation rates, k_N, that decrease to zero as a function of force, Fig. 5 *A*. The value k_N of the R1306Q A1 domain variant increases with force, as is characteristic of slip bonding. All of the variants have a common intermediate state dissociation rate, k_I, that increases with force. In Fig. 5 *B*, the binding probability, B_N, decreases to zero as a function of force and B_I increases with force up to a maximal probability defined by the intermediate. The force at which $B_N = B_I$ corresponds to the maximal bond lifetime of the native bound complex, τ_N, Fig. 4 *B*. Fig. 5, *C* and *D*, show that the flux through the native state, J_N decreases to zero as a function of force, whereas the flux through the intermediate state increases with force up to a maximal flux defined by k_I. The total flux, $J = J_N + J_I$, transitions from the native to intermediate state fluxes, which decrease at low force, J_N, to a minimum and increase at higher forces, J_I, in a similar manner to the selectins (22).

Analysis of the equilibrium properties of binding in the limit of zero force derived from the model in Fig. 3 illustrates these observations more clearly. Fig. 6 *A* shows the equilibrium dissociation rates as a function of the stability of the A1:GPIbα complex. The rate of dissociation from the intermediate, k_I^0, is constant and independent of the mutations in the A1 domain. However, the rate of dissociation from the native state, k_N^0, depends on the stability of the complex. As the stability of the A1:GPIbα complex increases, k_N^0 transitions from k_I^0 at low stability to a maximal rate of dissociation, $k_{N,\infty}^0$ at high stability as described by Eq. 9:

$$k_N^0\left(\Delta G_{NG\rightleftharpoons IG}^0\right) = \frac{k_I^0 + k_{N,\infty}^0 \exp\left(\frac{\partial \ln(k)}{\partial \Delta G_{NG\rightleftharpoons IG}^0}\left(\Delta G_{NG\rightleftharpoons IG}^0 - \Delta G_{NG\rightleftharpoons IG,1/2}^0\right)\right)}{1 + \exp\left(\frac{\partial \ln(k)}{\partial \Delta G_{NG\rightleftharpoons IG}^0}\left(\Delta G_{NG\rightleftharpoons IG}^0 - \Delta G_{NG\rightleftharpoons IG,1/2}^0\right)\right)} \quad . \tag{9}$$

$$\left(k_I^0 \le k_N^0 \le k_{N,\infty}^0\right)$$

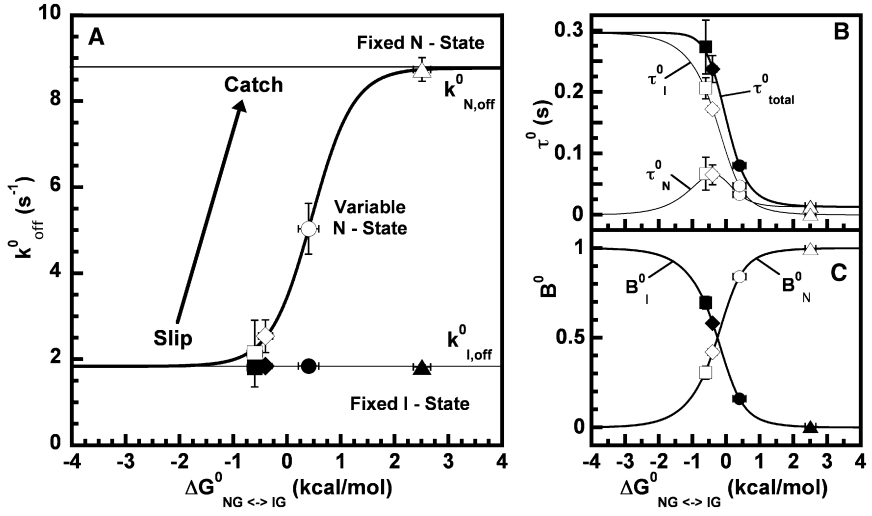

FIGURE 6 (*A*) Equilibrium (zero force) dissociation rates of GPIbα from the A1 domain native state (*open symbols*) and intermediate state (*solid symbols*) for each of the variants shown in Fig. 4 as a function of the thermodynamic stability of the A1:GPIbα complex ($\Delta G^0_{NG\rightleftharpoons IG}$). The k^0_N transitions from k^0_I at low stability to a maximal rate $k^0_{N,\ \infty}$ at high stability, as described by Eq. 9. The value $k^0_I = 1.83 \pm 0.03\ s^{-1}$, $k^0_{N,\ \infty} = 8.7 \pm 0.1\ s^{-1}$, $\partial \ln(k)/\partial \Delta G^0 = 2.7 \pm 0.3\ mol\ s^{-1}\ kcal^{-1}$, and $\Delta G^0_{1/2} = 0.51 \pm 0.05$ kcal mol^{-1}. (*B*) The resulting equilibrium native, intermediate, and total bond lifetimes. (*C*) The native and intermediate binding probability. R1306Q (*squares*), I1309V (*diamonds*), WT (*circles*), and G1324S (*triangles*).

The derivative, $\partial \ln(k)/\ \partial \Delta G^0_{NG\rightleftharpoons IG}$, is the cooperativity of the transition, $k = (k^0_N - k^0_I)/(k^0_{N,\ \infty} - k^0_N)$, and $\Delta G^0_{NG\rightleftharpoons IG,1/2}$ is the stability at which $k^0_N = (k^0_I + k^0_{N,\ \infty})/2$.

The effect of mutations on the thermodynamic stability of A1 alters the rates of dissociation of GPIbα from the native state without affecting the rate of dissociation from the intermediate. This observation is in line with our previous results from urea denaturation where the native state baselines of these A1 variants had different degrees of secondary structure, but unfolded to an identical intermediate secondary structure that was indifferent to the mutation (8). Relative to WT A1, G1324S increases k^0_N, whereas R1306Q and I1309V decrease k^0_N to the extent that $k^0_N \rightleftharpoons k^0_I$. From a thermodynamic perspective, the character of the native state of A1 is variable and the intermediate state is fixed with respect to the dissociation rates. The value k^0_N transitions from a fixed intermediate state character to a fixed native state character as a function of $\Delta G^0_{NG\rightleftharpoons IG}$ and the k^0_N for WT A1 is situated medially between these two extremes. This thermodynamic dependence of the dissociation rates is a defining feature of catch bonds that is likely to be caused by transient conformational fluctuations in the native state (23). At high stability, the dissociation of GPIbα from the low-affinity native conformation, $N_{A1}G$, is fast, and at low stability, the dissociation of GPIbα from the high-affinity intermediate conformation, $I_{A1}G$, is slow. Catch bonding only occurs when the rate of dissociation from the native state exceeds the rate of dissociation from the intermediate state, ($k^0_N > k^0_I$). Only when these rates become similar ($k^0_N \rightleftharpoons k^0_I$) does slip bonding occur.

An external verification of the model is that the equilibrium rate of dissociation from $N_{A1}G$ at zero force obtained from fitting the lifetime data agrees substantially with values previously obtained by different techniques. Our analysis results in a $k^0_N = 5.0 \pm 0.6 s^{-1}$ for WT A1 and $k^0_N = 2.5 \pm 0.4\ s^{-1}$ for I1309V A1. Using optical tweezers with A1 domain coated polystyrene beads and CHO cells expressing GPIb-IX, Arya et al. (24) obtained a $k^0 = 5.47 \pm 0.25\ s^{-1}$ for WT A1. Rolling velocity studies of GpIb-expressing CHO cells on A1 domain coated coverslips by Kumar et al. (25) resulted in a $k^0 = 5.66\ s^{-1}$ for WT A1. Laminar flow translocation assays of washed platelets on surface immobilized WT and I1309V A1 by Doggett et al. (26,27) resulted in $k^0 = 3.45 \pm 0.37\ s^{-1}$ and $k^0 = 0.56 \pm 0.02\ s^{-1}$, respectively. These results are systematically less than all the other published results by an average factor of $1.93 \pm 1.0\ s^{-1}$ for both variants of A1.

Substitution of Eq. 9 into Eqs. 7 and 8 in the limit of zero force defines the state specific bond lifetimes and probabilities of binding as a function of the stability of the complex (shown in Fig. 6, *B* and *C*). The total bond lifetime, equal to the sum of the state specific bond lifetimes, transitions from high to low as a function of $\Delta G^0_{NG\rightleftharpoons IG}$ and is paralleled by the state specific binding probabilities. At high stability, the probability of binding to the native state is maximal; however, it is balanced by a very fast rate of dissociation resulting in a low lifetime of the bond. At low stability, the probability of binding to the intermediate state is maximal, and the slow rate of dissociation enhances the bond lifetime. At stabilities within the transition region where the probabilities of binding to each state are similar, the native state specific bond lifetime is moderately enhanced, but still less than the lifetime of the intermediate state.

DISCUSSION

In our initial studies of the thermodynamics of A1 domain unfolding, it became apparent that the native to intermediate transition of the A1 domain could be representative of the conformational change that occurs in response to high shear stress (9). Further studies of the unfolding properties of the A1 domain containing Von Willebrand disease (VWD) type 2B gain of function and type 2M loss of function mutations

provided support for this mechanism (8). In these studies, the type 2B mutations shifted the equilibrium in favor of the intermediate conformation, whereas the type 2M mutation stabilized the native conformation of A1. Furthermore, we observed a distinct correlation between the force-dependent GPIbα binding properties of A1 and the thermodynamic stability of A1. A decrease in the stability of the A1 domain shifted the critical force of the catch bond to lower forces, resulting in an enhanced bond lifetime at equilibrium. Conversely, an increase in the stability of the A1 domain shifted the critical force of the catch bond to higher forces, resulting in a diminished bond lifetime at equilibrium. This inverse correlation between the force-dependent A1:GPIbα bond lifetimes and the stability of A1 suggested that the effect of shear forces on VWF shifts the equilibrium of the A1 domain in favor of the intermediate conformation, which could increase the affinity for GPIbα.

Here, we have reduced and carboxyamidated the disulfide bond of the A1 domain, RCAM A1, a chemical modification that releases conformational constraints and greatly stabilizes the intermediate state relative to the native state. There are two previous studies that investigated the structure of reduced and alkylated (R/A) A1 domain and its binding to GPIbα (28,29). In these studies, an intermediate structure of R/A A1 was observed via CD and fluorescence and this structural modification of A1 resulted in enhanced binding to platelets. R/A A1 domain was able to firmly adhere to platelets at low shear, but at higher shear its capacity to bind platelets was markedly diminished whereas the disulfide intact A1 domain firmly adhered to platelets most effectively at high shear. The results of these biological assays imply that the WT A1 domain unfolds to the intermediate at high shear and is able to catch-bond to platelets due to this conformational transition. In contrast, RCAM A1 binds platelets more efficiently at low shear and as the shear is increased, the bond slips and platelets are released.

We have demonstrated in this work that the A1 domain transition from native to intermediate increases the binding affinity for GPIbα and knowledge of the ΔG values for these processes establishes that the A1:GPIbα complex consists of a thermodynamic equilibrium between two distinct conformational states in which A1 is either native or intermediate. Given a force dependence of this equilibrium, we have quantified the allosteric catch-bond model for both WT and clinical variants of VWF. While it is beyond the scope of this study to compare the various proposed kinetic models of catch bonding, it should be noted that other two-state models of catch bonding are not able to capture the effects of both catch bonds and slip bonds that occur between A1 and GPIbα within the context of coupled thermodynamics of unfolding and binding (21,30,31). However, similar thermodynamic considerations have recently been suggested for selectin-mediated cell adhesion based on the crystal structures of both liganded and unliganded P-selectin conformations (32).

There are several important points to be learned from our analysis. First, binding of A1 to GPIbα at equilibrium favors the intermediate conformations of A1, i.e., $\Delta G^0_{NG \rightleftharpoons IG} < \Delta G^0_{N \rightleftharpoons I}$. This thermodynamic consequence results from the tighter binding affinity of the intermediate state of A1. Second, the effect of force on the A1:GPIbα interaction shifts the equilibrium in favor of the high affinity intermediate conformation resulting in prolonged lifetimes of the more thermodynamically stable A1 variants at higher forces. If the equilibrium stability is low, as is the case for R1306Q, the effect of force weakens the bond strength and shortens the bond lifetime at higher forces. Third, while the equilibrium dissociation rate from the intermediate state is fixed, the dissociation rate from the native state is dependent on the thermodynamic stability of the A1 domain in complex with GPIbα. This variable thermodynamic character of the native state dissociation rate could result from local structural fluctuations in A1 that transiently sample nonnative conformations that are prevalent within the intermediate state (23).

It should be noted that this analysis is from the perspective of the A1 domain, and does not include conformational aspects of the platelet GPIbα. Further studies of the thermodynamic properties of GPIbα are currently underway.

In summary, VWF circulates in a globular state in blood but it unfolds at high shear stress (6). This force unravels and elongates the VWF multimers, uncovers the A1 domain, and exposes the binding site for platelet GPIbα. Based on our analysis, we propose that subsequently, the binding of GPIbα to the A1 domain depends on the magnitude of the mechanical force of the bond that acts directly on the $N \rightleftharpoons I$ equilibrium of the exposed A1 domain structure. The WT A1 domain is strategically poised to take advantage of these transient shifts in equilibrium that are caused by shear forces due to its medial rate of dissociation. The changes in A1 stability caused by clinical VWD mutations result in minimal and maximal extremes of the dissociation rates that alter this critical sensitivity of VWF to the vascular shear forces. In addition, this analysis paves the way for more comprehensive investigations of the force-dependent binding properties of cellular adhesion proteins, which should include a foundation in thermodynamic principles.

SUPPORTING MATERIAL

Two schemes and 31 equations are available at http://www.biophysj.org/biophysj/supplemental/S0006-3495(10)00708-3.

This work was supported by the National Institutes of Health (grant No. HL72886 to M.A.C. and grant No. HL091020 to C.Z.), the Mary R. Gibson Foundation (to M.A.C. and M.A.), and the Baylor College of Medicine Thrombosis Research Training Grant (to M.A.).

REFERENCES

1. Ruggeri, Z. M. 1997. Mechanisms initiating platelet thrombus formation. *Thromb. Haemost.* 78:611–616.

2. Sadler, J. E. 1998. Biochemistry and genetics of von Willebrand factor. *Annu. Rev. Biochem.* 67:395–424.
3. Cruz, M. A., T. G. Diacovo, …, R. I. Handin. 2000. Mapping the glycoprotein Ib-binding site in the Von Willebrand Factor A1 domain. *J. Biol. Chem.* 275:19098–19105.
4. Dumas, J. J., R. Kumar, …, L. Mosyak. 2004. Crystal structure of the wild-type Von Willebrand Factor A1-glycoprotein Ibα complex reveals conformation differences with a complex bearing von Willebrand disease mutations. *J. Biol. Chem.* 279:23327–23334.
5. Siedlecki, C. A., B. J. Lestini, …, R. E. Marchant. 1996. Shear-dependent changes in the three-dimensional structure of human von Willebrand factor. *Blood.* 88:2939–2950.
6. Schneider, S. W., S. Nuschele, …, M. F. Schneider. 2007. Shear-induced unfolding triggers adhesion of von Willebrand factor fibers. *Proc. Natl. Acad. Sci. USA.* 104:7899–7903.
7. Arya, M., B. Anvari, …, J. A. López. 2002. Ultralarge multimers of von Willebrand factor form spontaneous high-strength bonds with the platelet glycoprotein Ib-IX complex: studies using optical tweezers. *Blood.* 99:3971–3977.
8. Auton, M., E. Sedlák, …, M. A. Cruz. 2009. Changes in thermodynamic stability of von Willebrand factor differentially affect the force-dependent binding to platelet GPIα. *Biophys. J.* 97:618–627.
9. Auton, M., M. A. Cruz, and J. Moake. 2007. Conformational stability and domain unfolding of the Von Willebrand factor A domains. *J. Mol. Biol.* 366:986–1000.
10. Yago, T., J. Lou, …, C. Zhu. 2008. Platelet glycoprotein Ibα forms catch bonds with human WT vWF but not with type 2B von Willebrand disease vWF. *J. Clin. Invest.* 118:3195–3207.
11. Morales, L. D., C. Martin, and M. A. Cruz. 2006. The interaction of von Willebrand factor-A1 domain with collagen: mutation G1324S (type 2M von Willebrand disease) impairs the conformational change in A1 domain induced by collagen. *J. Thromb. Haemost.* 4:417–425.
12. Qu, Y., C. L. Bolen, and D. W. Bolen. 1998. Osmolyte-driven contraction of a random coil protein. *Proc. Natl. Acad. Sci. USA.* 95:9268–9273.
13. Pace, C. N., F. Vajdos, …, T. Gray. 1995. How to measure and predict the molar absorption coefficient of a protein. *Protein Sci.* 4:2411–2423.
14. Kabsch, W., and C. Sander. 1983. Dictionary of protein secondary structure: pattern recognition of hydrogen-bonded and geometrical features. *Biopolymers.* 22:2577–2637.
15. Johnson, W. C. 1999. Analyzing protein circular dichroism spectra for accurate secondary structures. *Proteins.* 35:307–312.
16. Sreerama, N., and R. W. Woody. 2000. Estimation of protein secondary structure from circular dichroism spectra: comparison of CONTIN, SELCON, and CDSSTR methods with an expanded reference set. *Anal. Biochem.* 287:252–260.
17. Sreerama, N., S. Y. Venyaminov, and R. W. Woody. 1999. Estimation of the number of α-helical and β-strand segments in proteins using circular dichroism spectroscopy. *Protein Sci.* 8:370–380.
18. Martin, C., L. D. Morales, and M. A. Cruz. 2007. Purified A2 domain of VWF binds to the active conformation of VWF and blocks the interaction with platelet GPIbα. *J. Thromb. Haemost.* 5:1363–1370.
19. Cruz, M. A., R. I. Handin, and R. J. Wise. 1993. The interaction of the von Willebrand factor-A1 domain with platelet glycoprotein Ib/IX. The role of glycosylation and disulfide bonding in a monomeric recombinant A1 domain protein. *J. Biol. Chem.* 268:21238–21245.
20. Bell, G. I. 1978. Models for the specific adhesion of cells to cells. *Science.* 200:618–627.
21. Thomas, W., M. Forero, …, V. Vogel. 2006. Catch-bond model derived from allostery explains force-activated bacterial adhesion. *Biophys. J.* 90:753–764.
22. Springer, T. A. 2009. Structural basis for selectin mechanochemistry. *Proc. Natl. Acad. Sci. USA.* 106:91–96.
23. Whitten, S. T., B. García-Moreno E, and V. J. Hilser. 2005. Local conformational fluctuations can modulate the coupling between proton binding and global structural transitions in proteins. *Proc. Natl. Acad. Sci. USA.* 102:4282–4287.
24. Arya, M., A. B. Kolomeisky, …, B. Anvari. 2005. Dynamic force spectroscopy of glycoprotein Ib-IX and von Willebrand factor. *Biophys. J.* 88:4391–4401.
25. Kumar, R. A., J. F. Dong, …, L. V. McIntire. 2003. Kinetics of GPIbα-vWF-A1 tether bond under flow: effect of GPIbα mutations on the association and dissociation rates. *Biophys. J.* 85:4099–4109.
26. Doggett, T. A., G. Girdhar, …, T. G. Diacovo. 2003. Alterations in the intrinsic properties of the GPIbα-VWF tether bond define the kinetics of the platelet-type von Willebrand disease mutation, $Gly^{233}Val$. *Blood.* 102:152–160.
27. Doggett, T. A., G. Girdhar, …, T. G. Diacovo. 2002. Selectin-like kinetics and biomechanics promote rapid platelet adhesion in flow: the GPIb(α)-vWF tether bond. *Biophys. J.* 83:194–205.
28. Miyata, S., and Z. M. Ruggeri. 1999. Distinct structural attributes regulating von Willebrand factor A1 domain interaction with platelet glycoprotein Ibα under flow. *J. Biol. Chem.* 274:6586–6593.
29. Miyata, S., S. Goto, …, Z. M. Ruggeri. 1996. Conformational changes in the A1 domain of von Willebrand factor modulating the interaction with platelet glycoprotein Ibα. *J. Biol. Chem.* 271:9046–9053.
30. Barsegov, V., and D. Thirumalai. 2005. Dynamics of unbinding of cell adhesion molecules: transition from catch to slip bonds. *Proc. Natl. Acad. Sci. USA.* 102:1835–1839.
31. Evans, E., A. Leung, …, C. Zhu. 2004. Mechanical switching and coupling between two dissociation pathways in a P-selectin adhesion bond. *Proc. Natl. Acad. Sci. USA.* 101:11281–11286.
32. Waldron, T. T., and T. A. Springer. 2009. Transmission of allostery through the lectin domain in selectin-mediated cell adhesion. *Proc. Natl. Acad. Sci. USA.* 106:85–90.